LRP 712/01 October 2001

Effect of Specific Operating conditions on the Properties of LPPS Plasma Jets Expanding et Low Pressure

M. Gindrat, J.-L. Dorier, Ch. Hollenstein,
M. Loch, A. Refke, A. Salito, G. Barbezat

To be published in the
Proceedings of ITSC 2002
International Thermal Spray Conference
March 4-6, 2002, Essen, Germany

ISSN 0458-5895

Effect of specific operating conditions on the properties of LPPS plasma jets expanding at low pressure

M. Gindrat, J.-L. Dorier, Ch. Hollenstein, EPFL, CRPP, Lausanne, Switzerland
M. Loch, A. Refke, A. Salito, G. Barbezat, Sulzer Metco AG, Wohlen, Switzerland

The LPPS processes, which use DC plasma jets expanding at low pressure, are widely used for the deposition of various kinds of layers. The supersonic expansion of the plasma jet in a low-pressure environment requires special care in the operating conditions in order to obtain the desired properties of the flow, regarding powder injection and transport and plasma jet-surface interaction.
This paper presents measurements of the plasma jet properties for different chamber pressures. The torch is operated both in the over-expanded and under-expanded regimes, according to pressure measurements at the exit of the nozzle as a function of the backpressure. The topology of the expansion-compression zones of the plasma jet for the different operating pressures is inferred from imaging of the plasma jet. In addition, a modified enthalpy probe system is used to measure the specific enthalpy and the stagnation pressure profiles throughout the jet. Determination of the local free-stream jet parameters, such as the temperature and velocity, for the case of supersonic flow is made assuming an isentropic frozen stagnation process at the probe tip. For these calculations the pressure dependence of the equilibrium thermodynamic and transport properties is accounted for. Discussion on expanded jet rarefaction is made for chamber pressure below 20 mbar, in the light of plasma jet imaging and nozzle exit pressure measurements.

1 Introduction

Low Pressure Plasma Spraying (LPPS) or Vacuum Plasma Spraying (VPS) make use of plasma torches operated inside a vessel under reduced pressure. In contrast to Atmospheric Plasma Spraying (APS) these processes offer the advantage of a controlled atmosphere to avoid oxidation or contamination of the powders and sprayed deposit. This also allows an extension of the specific operation parameter space by controlling the chamber pressure.
Even though these LPPS processes are extensively used in a wide range of applications, only a few studies aiming to determine their plasma jet properties, either experimentally or numerically, have been reported to our knowledge. This is probably due to the great complexity of these high enthalpy, supersonic plasma jets, and to the inherent difficulties to set-up and interpret measurements when the jet is not in aerodynamic equilibrium. Most of the previous experimental investigations were limited to range of pressures down to 100 mbar [1, 2]. Several numerical simulations of supersonic DC plasma jets expanding in this pressure range have been made, but without [3] or with only limited [4] direct experimental validations. On the other hand, enthalpy probe measurements in supersonic plasma jets have been reported [5], but were limited to atmospheric pressure.
At lower chamber pressure (below 10 mbar) the plasma jet exhibits unconventional behavior related to very weak collisionality and large dimensions. In this regime a new process (LPPS Thin Film [6]) has been shown to rapidly deposit thin dense layers of metals or ceramics over large areas. Preliminary enthalpy probe measurements have been reported under these conditions [7], but these were interpreted using Local Thermodynamic Equilibrium (LTE) plasma properties which is doubtful at low pressure.
On the other hand, plasma jets expanding at very low pressures (below 1 mbar) and with low gas flow and power are used for PECVD of thin films [8]. These have been extensively investigated both experimentally and numerically, but are not relevant to the present investigations which cover the pressure range 2 to 100 mbar.
Hereafter we show the effect of chamber pressure on the jet expansion characteristics by imaging of the plasma jet structure and measurements of the nozzle exit pressure. Enthalpy probe measurements are presented for the high side of the pressure range investigated, and have been used to validate simulations presented in an associated paper [9].

2 Experiment

The plasma gun investigated is a Sulzer Metco F4-VB gun with a 6 / 12 mm diameter conical nozzle. It is mounted on a 2-axis displacement system inside a $2m^3$ vacuum vessel (Fig. 1A). The vessel pressure is regulated in the range 2 – 100 mbar by means of a 3-stage pumping system, equipped with pressure feedback controlled throttle valves. A dedicated enthalpy probe system, described elsewhere [7], allows measurement of the stagnation pressure and enthalpy in low pressure plasma jets. In this study, a 4.3/1.55 mm external/internal diameter probe is used. A fast, 12 bit CCD camera (*SensiCam Fast Shutter* from PCO), equipped with a 18 –108 mm zoom lens and a neutral density filter, is used to visualize the total plasma jet emission. It is also used to visualize the shock in front of the probe tip during enthalpy measurements [9]. The camera exposure time is 100 μs. The gun anode

(shown in Fig. 1B) has been modified to allow static pressure measurements inside and at the exit of the nozzle. This is used to determine whether the jet exhibits over-expanded or under-expanded flow. This also served as input for the simulation boundary conditions in reference [9].

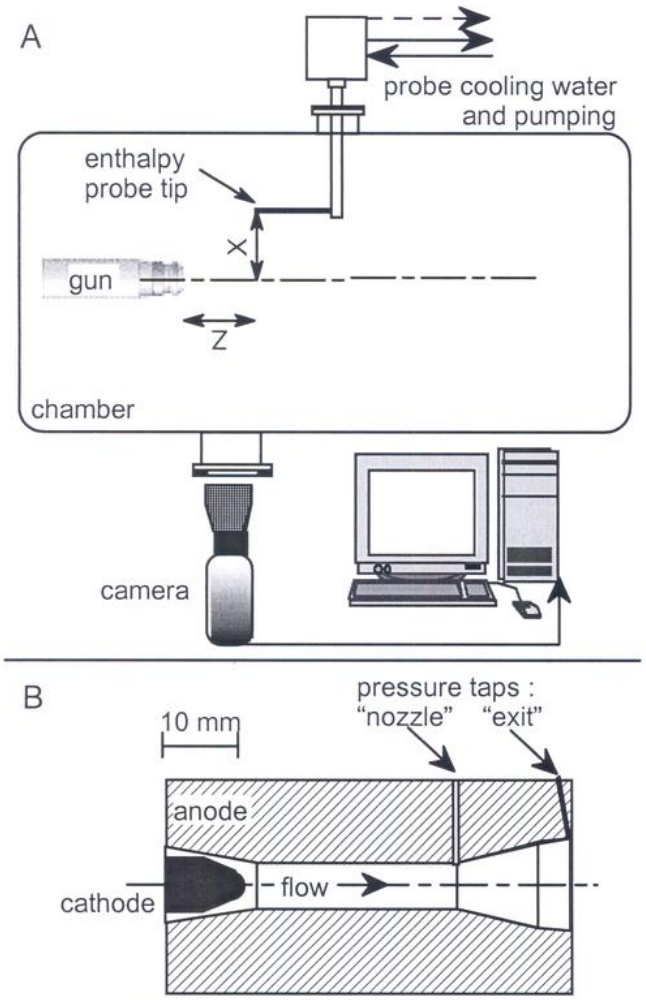

Fig. 1. Schematic top view of the experimental arrangement (A), and cross-section of the torch nozzle showing the pressure taps (B).

3 Results and discussion

The operating parameters' range investigated is 400-600 A current, 40 – 60 SLPM Ar flow and 2 – 100 mbar chamber pressure. No secondary gas such as H_2 has been used because this leads to re-strike of the arc inside the gun, and to an unsteady flow which is more complicated to characterize.

3.1 Chamber pressure effect on the jet topology

Figure 2 shows images of the plasma jet as a function of the chamber pressure in the range 20 – 100 mbar. At 100 mbar for example, the flow is over-expanded, as indicated by the oblique shocks which converge from the nozzle exit edges towards the jet axis. This is confirmed by a measured nozzle exit pressure smaller than the back pressure (figure 3). This over-expansion leads to a radial compression of the jet by the oblique shock wave originating from the nozzle exit edge. This builds up a compression zone around the jet axis, extending between 4.5 and 12 mm from the nozzle exit, visible as a bright emission patch. This compression leads to a local static pressure which exceeds the surrounding pressure and consequently the jet expands as it flows downstream. This is evidenced by an increased jet radius with weaker emission around z = 18 mm. This process of successive compression/expansion repeats further, until the local jet static pressure is in equilibrium with the surrounding pressure, due to viscous effects (around z = 60 mm in Fig. 2). A more detailed description of these plasma jet over-expansion phenomena can be found in reference [9].

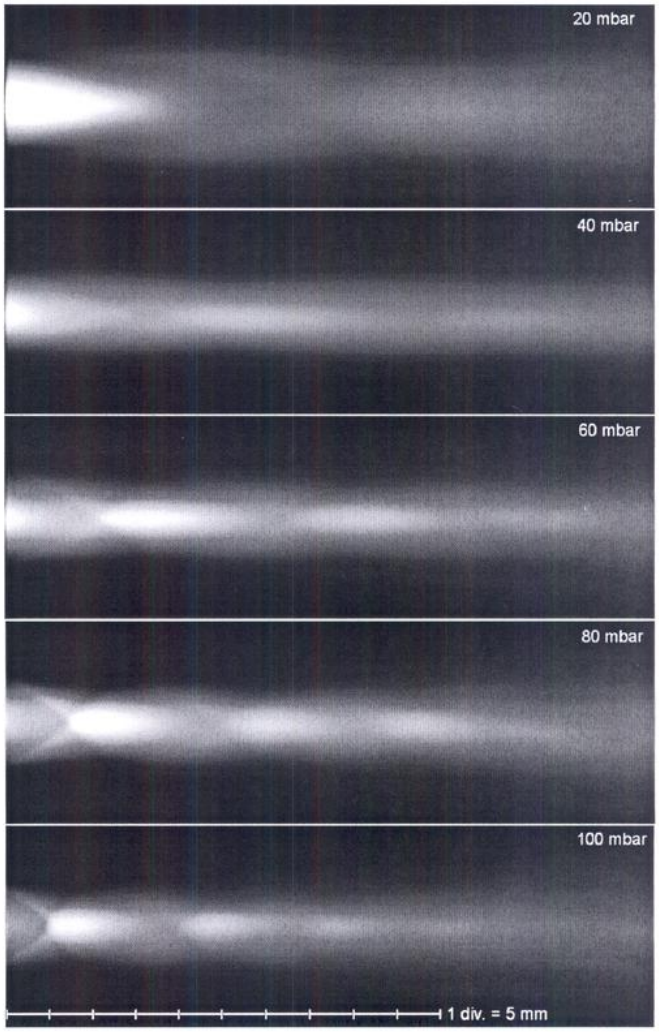

Fig. 2. Images of the plasma jet at different chamber pressures. Torch parameters : 600A, 60 SLPM Ar.

As the chamber pressure is reduced, these successive compressions/expansions are stretched, and build up farther from the nozzle exit. This is mainly because of the absolute pressure reduction: the jet needs more distance to equilibrate pressure as evidenced in Fig. 2 for 80 and 60 mbar. Around 45 mbar chamber pressure (for the conditions of Fig. 2), both exit and chamber pressures are equal which corresponds to the so-called "design pressure" (indicated by arrows on Fig. 3). The jet static pressure is in equi-

librium with the surrounding pressure and no longer exhibits successive compressions/expansions. In Fig. 2, the jet at 40 mbar is close to this situation and very weak shock structure is visible. Since the jet properties are the most homogeneous at the "design pressure", it might be worth tuning the chamber pressure to approach this regime as close as possible for best spraying conditions. However, it should be noted that the "design pressure" strongly depends on the torch parameters, as show in Fig. 3 for 400 A, 40 SLPM. In fact, Fig 4 confirms that the jet flow is still over-expanded at 40 mbar chamber pressure in that case.

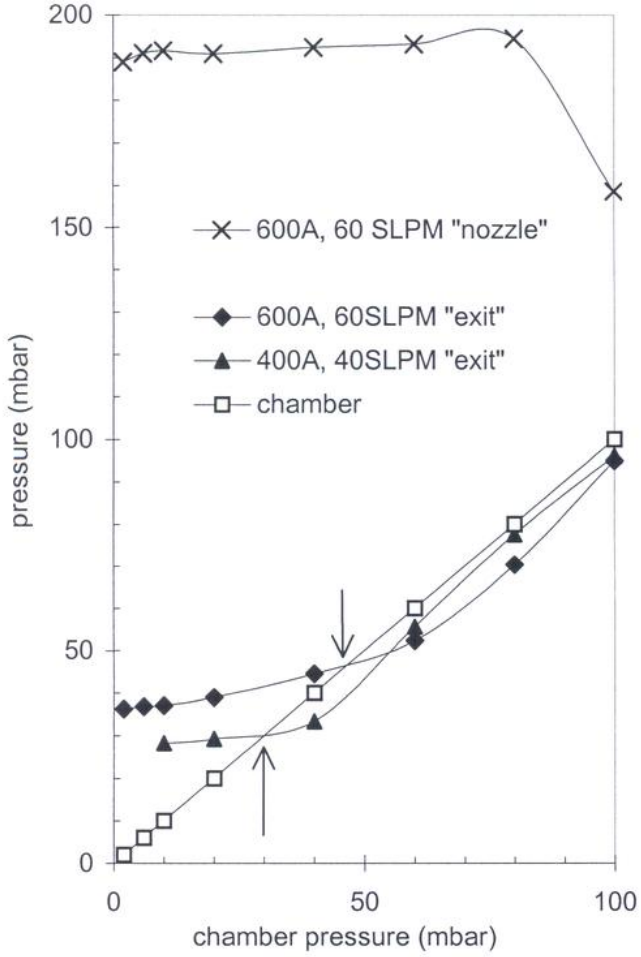

Fig. 3. Dependence on the chamber pressure of "nozzle" and "exit" pressures (referred in Fig.1B) for two torch parameters. (Arrows indicate the "design pressure").

Figure 3 also shows that the pressure measured at the beginning of the conical section of the nozzle ("nozzle" pressure tap in Fig. 1B) is almost independent of the chamber pressure below 80 mbar. Therefore, here, the sonic transition (M = 1) of the flow takes place at the end of the cylindrical section of the nozzle, whereas for chamber pressures above 80 mbar it occurs in the conical part. This means that the geometry of the nozzle, for given torch operating conditions, also influences the value of the "design pressure".
If the chamber pressure is further reduced below 45 mbar, the jet progressively switches to an under-expanded flow. This starts by an expansion at the nozzle exit as evidenced by the increased jet radius and the strong emission reduction (e.g between z=20 and 40 mm at 20 mbar in Fig. 2 or 5).

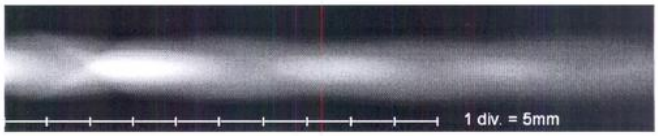

Fig. 4. Image of the plasma jet showing over-expansion at 40 mbar for 400 A torch current and 40 SLPM Ar flow.

Figure 5 shows images of the plasma jet for pressures below 20 mbar. These under-expanded jets are characterized by a hot and dense plume exiting the nozzle, whose length increases as the chamber pressure decreases. This plume is followed by an expansion with a significant drop in temperature and pressure close to the jet axis. The edges of this first expansion zone are brighter because barrel shocks are formed by reflection of the expanding flow from the cold, dense surrounding gas. This leads to a compression and converts part of the kinetic energy into thermal energy. There is a local increase of the temperature and density, and hence of the light emission. The flow is then redirected towards the axis and forms the first compression zone (e.g. between z = 60 and 90 mm at 10 mbar on Fig. 5).
Subsequent expansions / compressions occur until the local jet pressure equilibrates with the chamber pressure, as shown in Fig. 5 for the 20 and 10 mbar cases. For lower chamber pressures, the flow structure, as evidenced by the plasma emission, looks different and can no longer be described by classical gas dynamics.

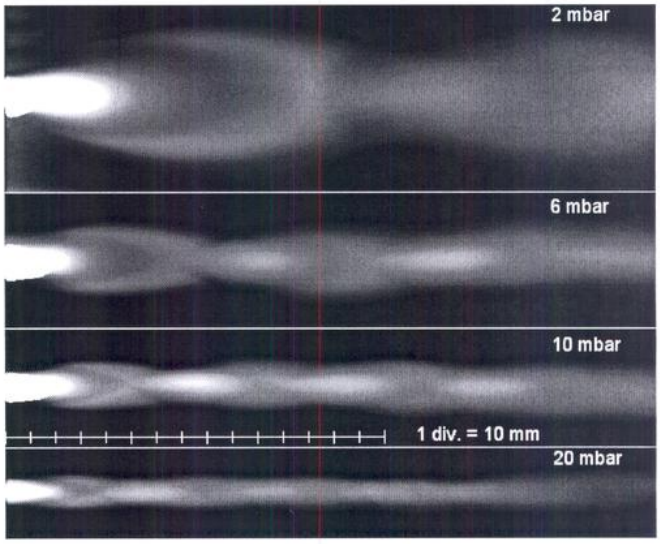

Fig. 5. Images of the plasma jet for pressures below 20 mbar. Torch parameters : 50 SLPM Ar, 500 A current.

Figure 3 shows that the nozzle exit pressure does not continually fall as the chamber pressure is reduced in the under-expanded flow regime. It even tends to saturate for the lowest achievable chamber pressures.

Muntz et al. [10] have characterized exhaust jet rarefaction by the following parameter ξ:

$$\xi = D\frac{\sqrt{p_e p_c}}{T} \qquad (1)$$

where D is the nozzle exit diameter (cm), p_e and p_c (dyne/cm^2) the exit and chamber pressures respectively, and T the mean temperature (K). Figure 6 represents ξ as a function of chamber pressure, calculated using the measured exit pressures of Fig. 3 and assuming T = 5000 K and D = 12 mm.

For ξ higher than about 5, the flow is in the continuum regime, which corresponds to chamber pressures above approximately 15 mbar in our case. Here the flow in the expansion region at the nozzle exit consists of an internal inviscid core surrounded by barrel shocks and a mixing, turbulent zone. For pressures below 15 mbar, the rarefaction parameter is characteristic of a transition flow regime, where the shocks become progressively thicker, as evidenced by the images at 6 and 2 mbar in Fig. 5. In some cases of strong under-expansion, a Mach disk shock can be formed downstream of the first expansion cell [8]. If the pressure was further decreased, the flow would have progressively entered the so-called "scattering regime" around ξ<1, which is characterized by the disappearance of well-delimited shock structures.

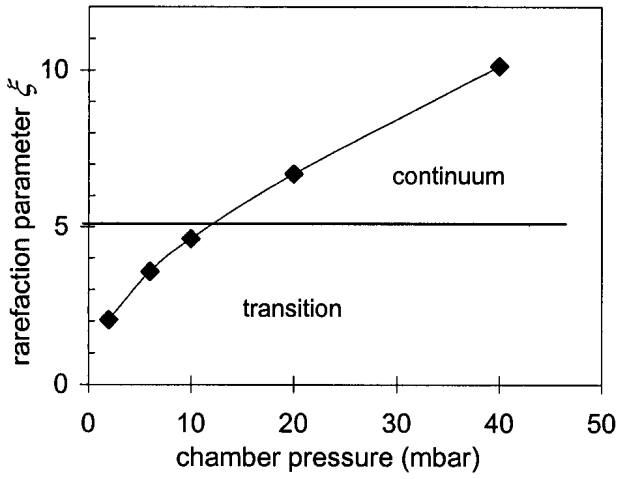

Fig. 6. Effect of chamber pressure on the rarefaction parameter ξ. Torch parameters 600A, 60 SLPM Ar.

3.2 Enthalpy probe measurements

Figure 7 shows radial profiles of the measured stagnation pressure and total enthalpy at axial positions corresponding to successive expansion and compression zones in the 100 mbar jet shown in Fig. 2.

These raw data are used to validate the 2D fluid model presented in reference [9]. It should be pointed out that the indicated axial positions correspond to the probe tip positions, which are slightly downstream of the points where the measured jet properties take place (upstream of the shock formed in front of the tip). In fact, a non-negligible shock-to-probe tip distance (up to 3 mm, depending on the axial position from the nozzle exit) has to be accounted for. Specific problems related to enthalpy probe measurements in supersonic flows which are in aerodynamic non-equilibrium are discussed in reference [9].

In Figure 7A, the stagnation pressure profiles are maximum on axis in the compression zones (z = 26 and 40 mm) whereas they are hollow and broader in the expansion zones. This reflects the jet topology depicted in Fig. 2. At z = 18 mm the pressure profile drops significantly on axis. This is probably because the flow crosses a Mach reflection at z = 4.5 mm around the axis (see Fig. 2 and reference [9]). This is a strong, non-isentropic normal shock which reduces the dynamic pressure. The stagnation enthalpy profiles are always maximum on axis because this is the region of maximum temperature and velocity, but they are also broader in the expansion regions.

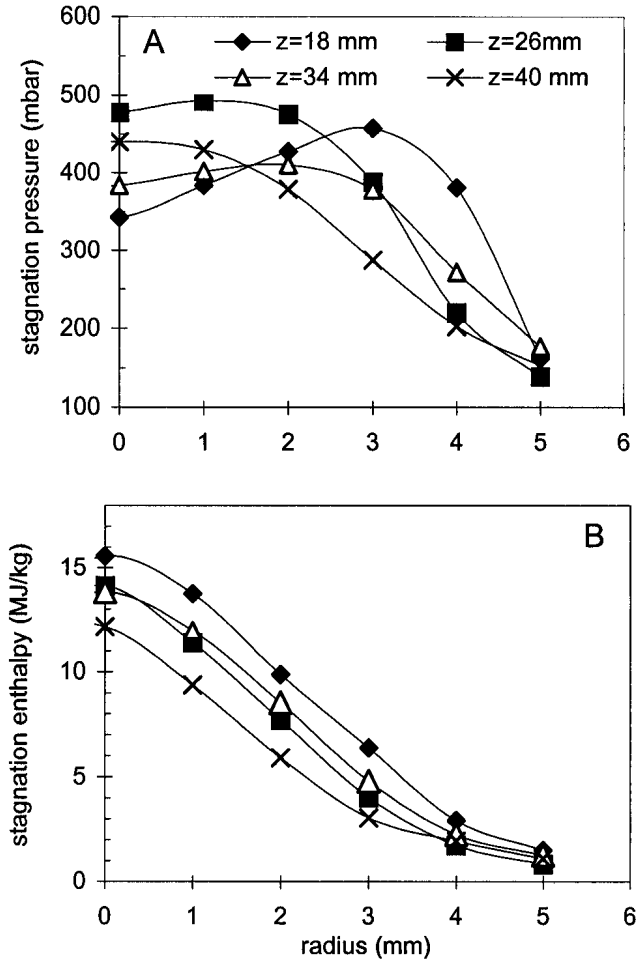

Fig. 7. Measured radial profiles of the stagnation pressure (A) and total enthalpy (B) at different axial positions under the conditions of Fig. 2 at 100 mbar.

Figure 8 shows the calculated temperature and velocity radial profiles using the iterative procedure described in reference [7], assuming isentropic stagnation process at the probe tip. For these calculations the pressure dependence of the thermodynamic properties of the jet, such as $\gamma = c_p/c_v$, sound velocity and specific enthalpy, are taken into account and calculated assuming LTE. The determination of the local Mach number, and hence of the velocity, depends on the ratio of stagnation (total) to static pressure. Since

the local static pressure is unknown and can be fairly different from the chamber pressure through the successive compression / expansions of the jet, we used the static pressure profiles from the simulation of reference [9] for the present calculations.
Both the temperature and velocity profiles of Fig. 8 are broader in the expansion regions in agreement with the jet topology of Fig. 2. But their values on axis do not drop substantially downstream, over the axial region investigated here. This reveals an efficient isolation of the jet core from the surroundings, as regards heat and momentum losses. However, the area-integrated heat flux throughout the jet cross section decreases from 8 kW at 18 mm down to 5 kW, at 40 mm for a net torch power of 10.5 kW. This drop of the integrated heat flux and the shapes of the radial profiles of Fig. 8 show that the jet is cooled and slowed down from the mixing zone at the edges, outside the barrel shocks. This differs from subsonic plasma jets which experience turbulent surrounding gas engulfment and cooling straight through the core. Here the core jet flow is supersonic and non-turbulent over the whole region investigated, with Mach numbers approaching 2 on axis and falling down to around 0.7 at the edges of the measured profiles.

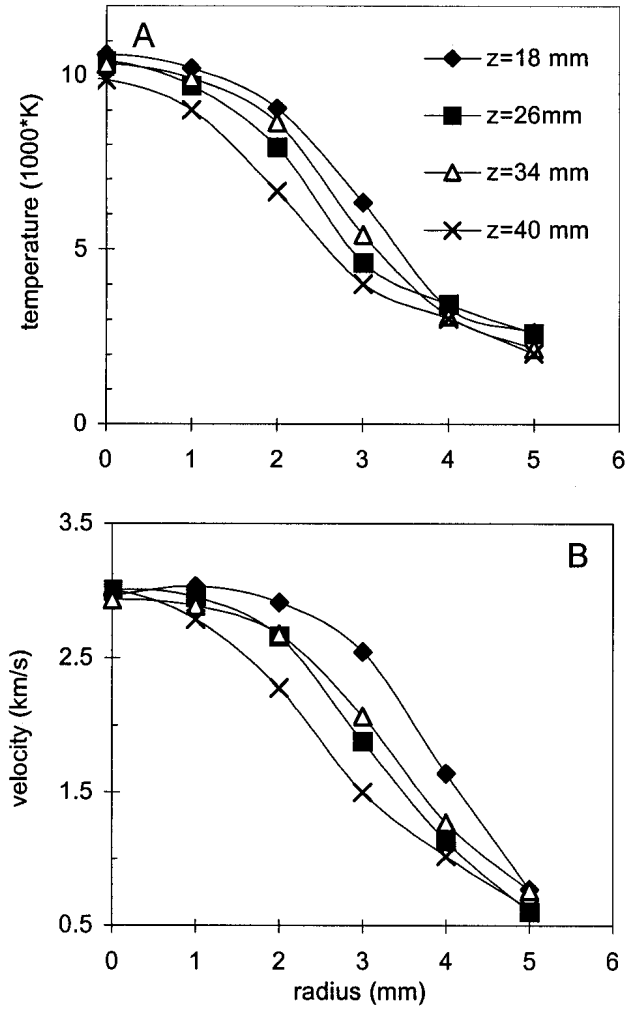

Fig. 8. Temperature (A) and velocity (B) radial profiles at different axial positions determined from the measured data of Fig. 7.

We have been able to perform total enthalpy and stagnation pressure measurements at chamber pressures down to 20 mbar with the present arrangement. Figure 9 shows radial profiles taken at two axial positions corresponding to the middle of the first expansion zone (z = 30 mm) and of the first compression zone (z = 53 mm), according to Fig. 2 for the 20 mbar case.
However the actual iterative procedure used to calculate the free stream jet properties using the measured total enthalpy and stagnation pressure failed for positions off jet axis. At these positions, the calculated kinetic component of the total enthalpy, given by half of the calculated squared velocity, exceeds the measured total enthalpy already at the first iteration. This leads to unphysical negative free stream enthalpies. In the following we will discuss the possible causes of this problem.

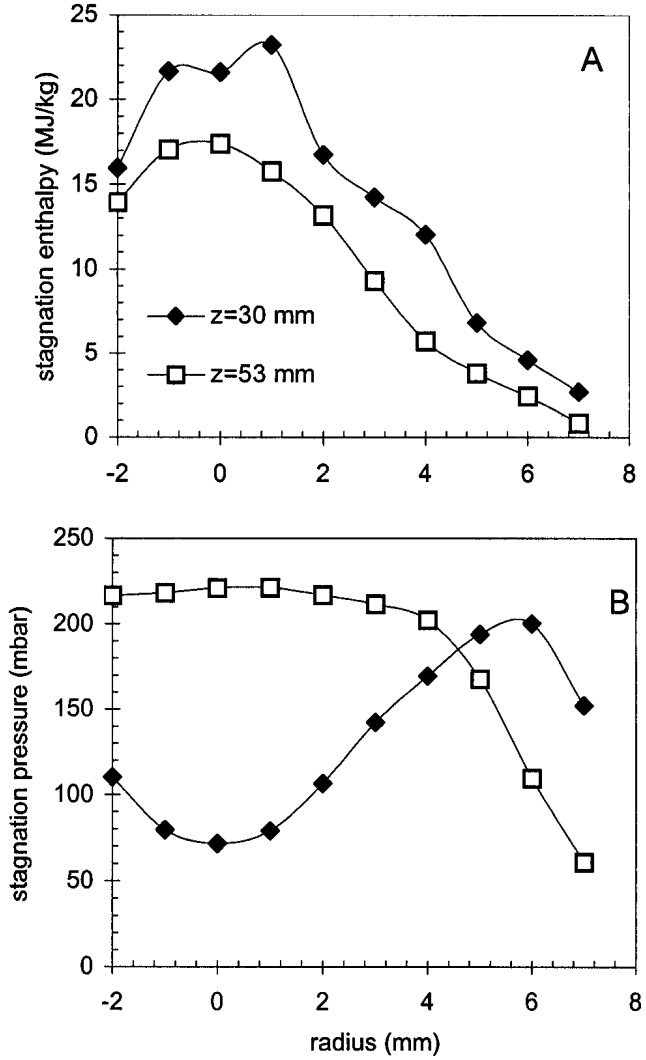

Fig. 9. Measured total enthalpy (A) and stagnation pressure (B) radial profiles at two axial positions in the conditions of Fig. 2 at 20 mbar chamber pressure.

First, the local static pressure at the measurement point is difficult to determine with a sufficient accuracy, because of the large pressure gradients, exacerbated in under-expanded jets at low chamber pressures [9]. Second the jet is deflected by the probe. When the probe is on the jet axis, the shock has a normal com-

ponent at the tip axis, but is oblique at the edges, as shown in reference [9]. When the probe is off jet axis the shock might no longer be normal at the measurement orifice. This leads to a spurious measurement of the stagnation pressure, whereas the total enthalpy is less affected because of conservation laws. Moreover, the expression which relates the Mach number to the ratio of stagnation to static pressures is applicable only if the shock is normal. This jet deflection can be suspected by inspection of Fig. 9 which shows very broad stagnation pressure profiles compared with enthalpy profiles.
Finally, we assumed LTE jet conditions, which might break down at these low pressures [11].

3 Conclusions

A DC plasma torch expanding in a reduced pressure environment has been investigated using imaging of the jet emission topology and enthalpy probe measurements. The most prominent physical mechanisms governing the flow in this situation have been described. A transition from an over-expanded to an under-expanded flow regime has been evidenced by a change in the jet topology and measurements of the nozzle exit pressure as a function of the chamber pressure. The sensitivity of this transition pressure (the "design pressure") on the torch operating parameters has been underlined, with regards to optimum spraying conditions.
The rarefaction of the jet has been characterized by an estimation of a rarefaction parameter depending on exit and chamber pressures. At low chamber pressures (around 15 mbar), a progressive change from a continuum to a transition flow regime has been shown by the thickening of the shock structures.
Measurements of the stagnation enthalpy and pressure with a dedicated enthalpy probe system have been performed. An iterative procedure using the LTE, pressure-dependent thermodynamic jet properties and simulated static pressure profiles has been applied. This allowed to calculate the free stream jet temperature and velocity throughout successive compression and expansion regions of the jet at 100 mbar. However, this procedure seems not to be applicable off axis of plasma jets operated at pressures below 50 mbar. It is suspected that, here, the shock in front of the probe orifice becomes oblique, deflects the jet, and leads to erroneous stagnation pressure measurements.
Further work is needed to account for the peculiarities of enthalpy probe measurements in supersonic jets which are in aerodynamic non-equilibrium.

Acknowledgments

The authors are indebted to Professor Bertrand Jodoin for his valuable contribution to the present work and for the fruitful collaboration. We also thank Dr. Laurent Sansonnens for his advice and for the calculations of thermodynamic plasma properties.
This work is funded by a CTI Swiss Federal Research Projet No. KTI 4403.1KTS.

References

[1] H. J. Kim and S. H. Hong, "Comparative measurements of thermal plasma jet characteristics in atmospheric and low pressure plasma spraying", IEEE Transactions on Plasma Science 23 (5), 852, (1995).

[2] M. Hollenstein, M. Rahmane, and M. I. Boulos, "Aerodynamic study of the supersonic induction plasma jet", Proc. of the 14th Int. Symposium on Plasma Chemistry, Prague, Czech Republic, p.257, (1999).

[3] Peng Han and Xi Chen, "Modeling of the supersonic argon plasma jet at low gas pressure environment",Thin Solid Films **390**, 181-185, (2001).

[4] S.E.Selezneva, M. Rajabian, D. Gravelle and M. Boulos, "Study of the structure and deviation from equilibrium in direct current supersonic plasma jets", J. Phys. D : Appl. Phys. **34**, 2862, (2001).

[5] J. R. Fincke, W. D. Swank, S. C. Snider, and D. C. Haggard, "Enthalpy probe performance in compressible thermal plasma jets", Rev. Sci. Instrum. 64 (12), 3585, (1993).

[6] M. Loch, and G. Barbezat, "Characteristics and Potential Application of Thermally Sprayed Thin Film Coatings", "Thermal Spray: Surface Engineering via Applied Research", Ed. C. C. Berndt, Pub. ASM International, Material Park, OH, USA, 1141, (2000).

[7] J.-L. Dorier, M. Gindrat, Ch. Hollenstein, M. Loch, A. Refke, A. Salito, and G. Barbezat, "Plasma jet properties in a new spraying process at low pressure for large are thin film deposition", in Thermal Spray 2001 : New Surfaces for a New Millenium, Ed. C.C. Berndt, K.A. Khor, E. Lugscheider, Pub. ASM INternational, Materials Park, OH, USA, 2001, p.759-764

[8] M. C. M. van de Sanden, R. J. Severens, W. M. M. Kessels, R. F. G. Meulenbroeks and D. C. Schram, J. Appl. Phys. 84, 2426, (1998); J. Appl. Phys. 85, 1243, (1999) and references therein.

[9] B. Jodoin, J.-L. Dorier, M. Gindrat, C. Hollenstein, M. Loch and G. Barbezat, "Modelling and diagnostics of a supersonic DC plasma jet expanding at low pressure", This conference.

[10] E.P. Muntz, B.B. Hamel and B.L. Maguire, "Some characteristics of exhaust plume rarefaction", AIAA Journal **8(9)**, 1651, (1970).

[11] N. Singh, M. Razafinimanana, and A. Gleizes, "The effect of pressure on a plasma plume: temperature and electron density measurements", J. Phys. D: Appl. Phys. 31, 2921, (1998).